Overlimiting current in non-uniform arrays of microchannels: Recirculating flow and anti-crystallization

Hyekyung Lee[1†,ǂ], Seoyun Sohn[1†,‡], Shima Alizadeh[2], Soonhyun Kwon[1], Tae Jin Kim[3], Seung-min Park[4], Hyongsok Tom Soh[4,5], Ali Mani[2*] and Sung Jae Kim[1,6,7*]

[1]*Department of Electrical and Computer Engineering, Seoul National University, Seoul 08826, Republic of Korea*

[2]*Department of Mechanical Engineering, Stanford University, Stanford 94305, USA*

[3]*Department of Radiation Oncology, Stanford University, Stanford 94305, USA*

[4]*Department of Radiology, Stanford University, Stanford 94305, USA*

[5]*Department of Electrical Engineering, Stanford University, Stanford 94305, USA*

[6]*Nano System Institute, Seoul National University, Seoul 08826, Republic of Korea*

[7]*Inter-university Semiconductor Research Center, Seoul National University, Seoul 08826, Republic of Korea*

† These authors contributed equally.
Current affiliation: ǂNational Agenda Research Division, Korea Institute of Science and Technology, Seoul 02792, Republic of Korea and ‡Institute of Materials Research, Helmholtz-Zentrum Geesthacht, Geesthacht 21502, Germany
*Correspondence should be addressed to Prof. Ali Mani and Prof. Sung Jae Kim
E-mail: (Ali Mani) alimani@stanford.edu, (Sung Jae Kim) gates@snu.ac.kr

SI Note 1. Voltage sweep rate dependency

In the I-V measurement (Figure 2 in main text), an overshoot appeared. This was attributed a strong dependency to the voltage sweep rate (S). Its relationship was reported as $i_{peak} \sim S^{0.5}$.[1, 2] However, the magnitude of the measured overlimiting conductance is much less sensitive to the voltage sweeping rate as shown in SI Figure 1, since this regime involves a longer time than the limiting regime time, and thus CP can fully develop. Therefore, experiment in SI Figure 3 supported the voltage sweep rate in our explored regime does neither change the measured OLC nor it affects our end conclusions.

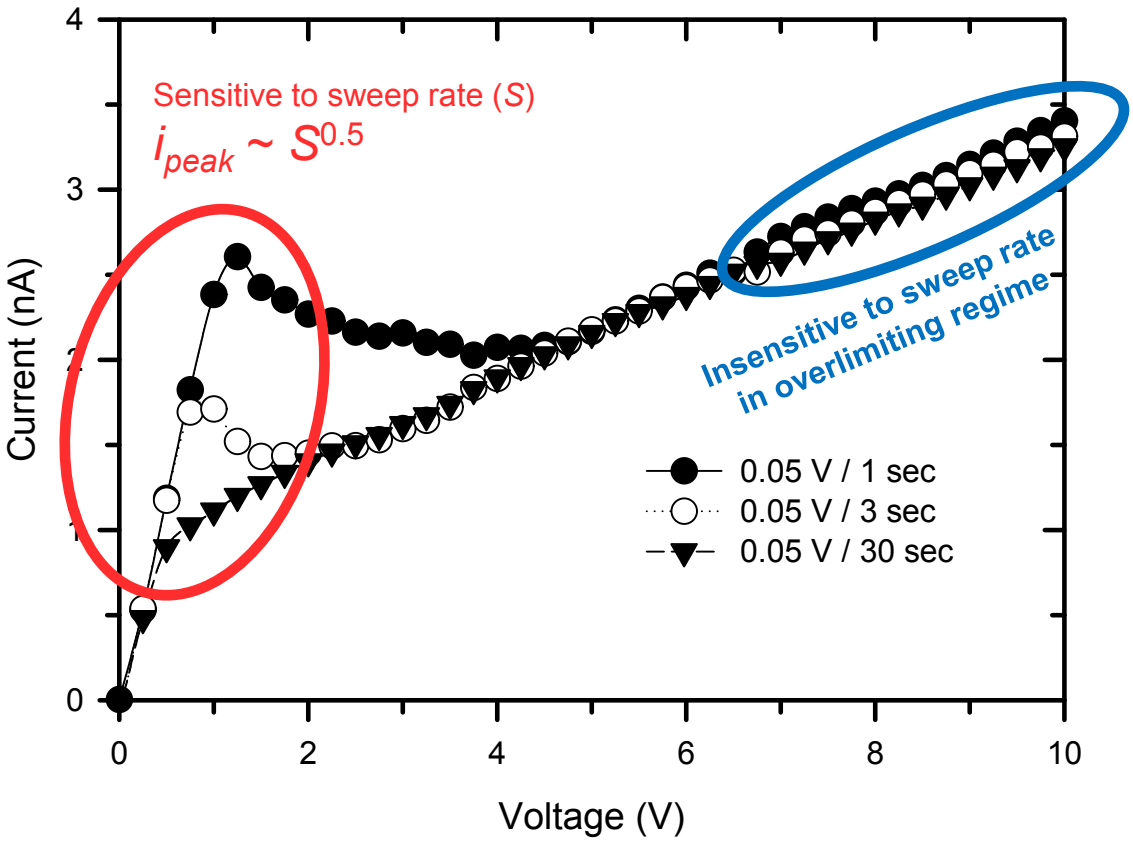

SI Figure 1. I-V responses with varying sweeping rates. It can confirm that limiting current values can be a function of sweeping rate, but the overlimiting current values are insensitive to the sweeping rate.

SI Note 2. Analytical solution of recirculation flow

First of all, the numerical values of the friction factor, $f(h_i)$, are as follows.

h_i = [0.5 1.5 2.5 3.5 4.5 5.5 6.5 7.5 8.5 9.5 10.5 11.5 12.5 13.5 14.5] and $f(h_i)$ = [0.9560 0.8731 0.7894 0.7061 0.6255 0.5500 0.4817 0.4215 0.3692 0.3243 0.2859 0.2532 0.2252 0.2012 0.1806].

To satisfy the continuity condition, the sum of pressure-driven flow should be the sum of electroosmotic flow in each channel. Thus,

$$\begin{aligned} & Q_{p_w} + Q_{p_n} = Q_{EO_w} + Q_{EO_n} \\ \Leftrightarrow & \frac{\Delta P}{12\mu L}(h_w{}^3 f(h_w) + h_n{}^3 f(h_n))d = \frac{\varepsilon(-\zeta)|\mathbf{E}|hd}{\mu} \\ \Leftrightarrow & \frac{\Delta P}{12\mu L} = \frac{\varepsilon(-\zeta)|\mathbf{E}|}{\mu}\frac{h}{h_w{}^3 f(h_w) + h_n{}^3 f(h_n)}. \end{aligned} \tag{S1}$$

Then, the net flow rate (Q_{rec}) in wide channel is calculated as

$$\begin{aligned} & Q_{rec} = Q_{P_w} - Q_{EO_w} \\ & = \frac{\Delta P}{12\mu L} h_w{}^3 f(h_w)d - \frac{\varepsilon(-\zeta)|\mathbf{E}|h_w d}{\mu} \\ & = \frac{\varepsilon(-\zeta)|\mathbf{E}|}{\mu}\frac{h}{h_w{}^3 f(h_w) + h_n{}^3 f(h_n)} h_w{}^3 f(h_w)d - \frac{\varepsilon(-\zeta)|\mathbf{E}|h_w d}{\mu} \\ & = \frac{\varepsilon(-\zeta)Vhd}{\mu L}\left[\frac{\left(\frac{h_w}{h}\right)^3 f(h_w)}{\left(\frac{h_w}{h}\right)^3 f(h_w) + \left(\frac{h_n}{h}\right)^3 f(h_n)} - \frac{h_w}{h}\right]. \end{aligned} \tag{S2}$$

(S2) is plotted as a function of h_w in $0 < h_w < 15$ μm in SI Figure 2. Net flow would vanish at the uniform cases of (h_w, h_n) = (7.5 μm, 7.5 μm), (0 μm, 15 μm) and (15 μm, 0 μm), while local maximum appears at (11.3 μm, 3.7 μm). The local minimum is the local maximum in reverse circulation at (3.7 μm, 11.3 μm).

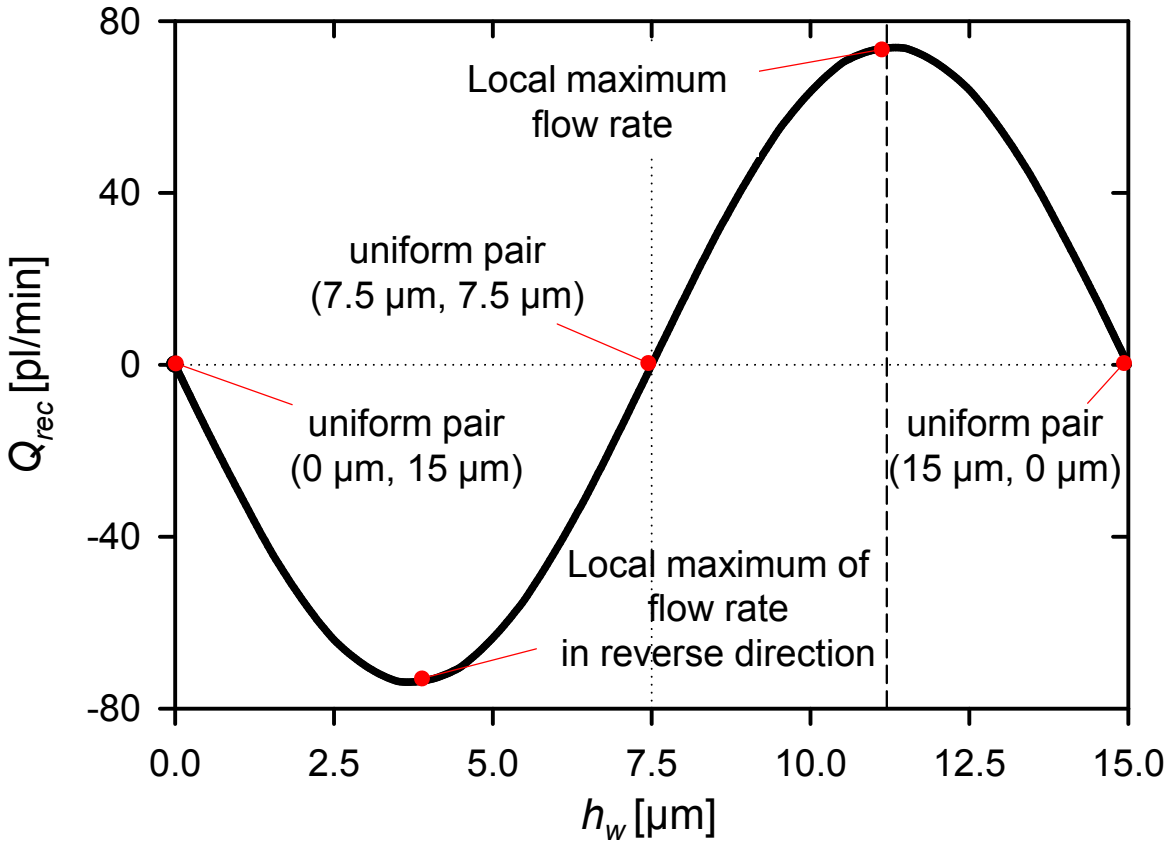

SI Figure 2. Plot of calculated net flow obtained from equation (S2) as a function of h_w.

SI Note 3. Numerical analysis of ionic current through membrane

We conduct a theoretical analysis for electrolyte concentration and ionic current through a perm-selective membrane associated with a non-uniform microchannel pair. The domain is divided into 4 regions as shown in SI Figure 3(a), which are labeled as reservoir 1, narrow, wide and reservoir 2. Note that this simulation is conducted only for one pair of narrow-wide channels, while actual experiment is performed in 33 pairs of narrow-wide channels. Here, V_{app} and V_{cp} are the external voltage to the entire channel and the actual voltage applied only to the wide and narrow channels. l_{res1}, l_{cp} and l_{res2} are the length of the region upstream of the CP region, the region that is divided by smaller channels and the short region downstream of the channels.

Each region has normalized governing equations of time-dependent diffusion equation in reservoir1 and reservoir2 and time-dependent diffusion convection equation in narrow and wide region as shown in SI Figure 3(b). Electroneutrality is assumed in entire region to eliminate drift term in governing equations. The convection in narrow (u_n) and wide (u_w) regime is given by $Q_{rec}/h_n d$ and $Q_{rec}/h_w d$, respectively. In the diagram, c_{res1}, c_{cp_n}, c_{cp_w} and c_{res2} are the electrolyte concentration in each region. D is the diffusivity of ions. The boundary conditions are as depicted. The matching conditions at each interface are realized in the code using the same finite volume flux schemes for the interior faces of the connecting channel, with a modification to account for multiple boundary cells and weighting fluxes with faced areas. One-dimensional finite difference solver is programmed using MATLAB. By a proper convergence test, appropriate total simulation time is set as shown in SI Figure 3(c).

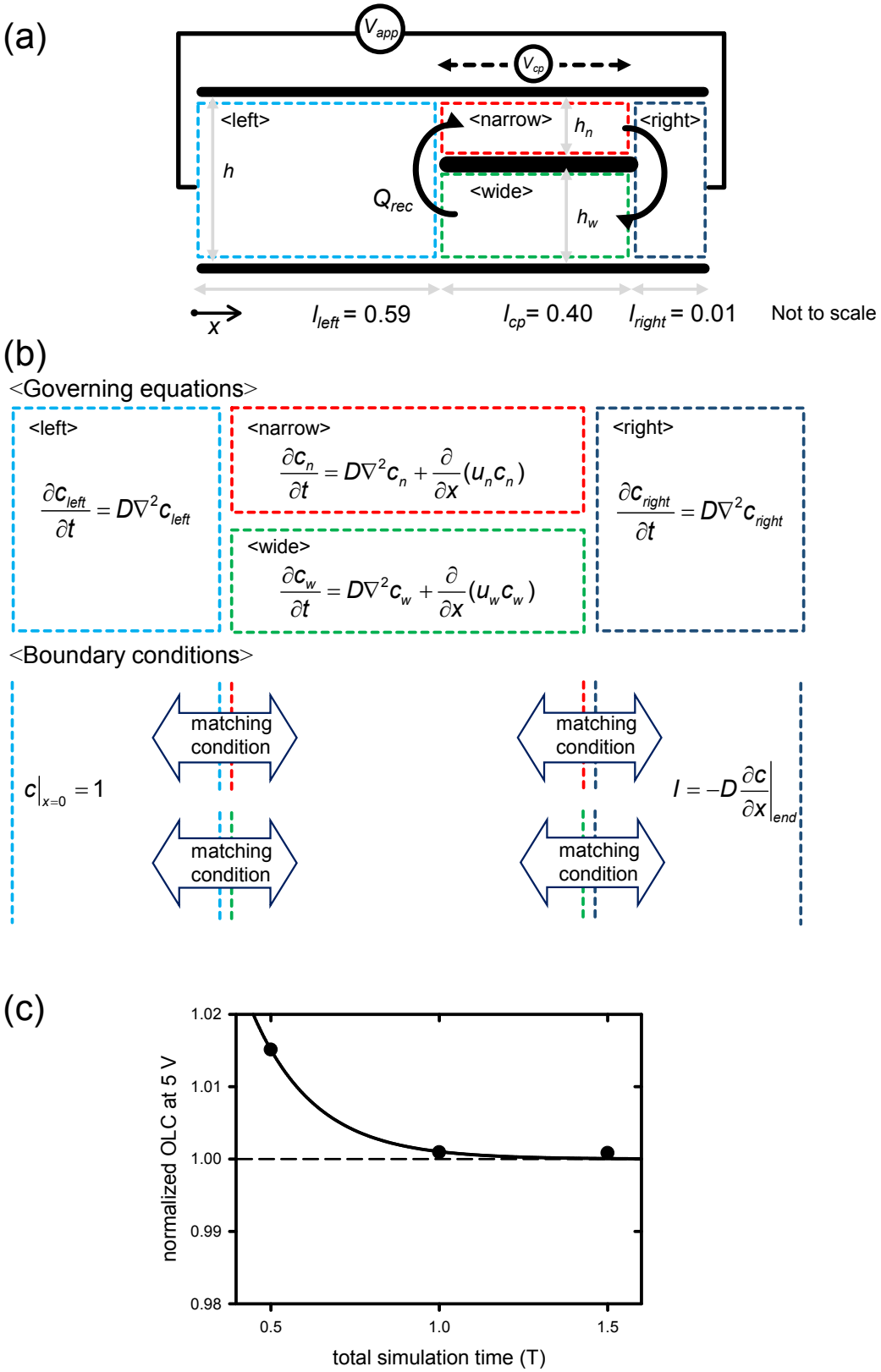

SI Figure 3. (a) The computational domain of non-uniform microchannel network. This domain includes only one pair of network. (b) Governing equations and boundary conditions in each region. (c) Convergence test of simulation time.

For the convenience, equivalent circuit model is introduced so that the current I and V_{cp} can be obtained as follows;

$$I(t) = \frac{V_{app}}{R_{res1} + \frac{1}{\frac{1}{R_n} + \frac{1}{R_w}} + R_{res2}} \quad \text{and} \quad V_{cp} = V_{app} \frac{\frac{1}{\frac{1}{R_n} + \frac{1}{R_w}}}{R_{res1} + \frac{1}{\frac{1}{R_n} + \frac{1}{R_w}} + R_{res2}}. \tag{S3}$$

where

$$R_{res1} = \int \frac{1}{c_{res1}} dx,\ R_n = \int \frac{h}{h_n} \frac{1}{c_{cp\_n}} dx,\ R_w = \int \frac{h}{h_w} \frac{1}{c_{cp\_w}} dx \text{ and } R_{res2} = \int \frac{1}{c_{res2}} dx. \tag{S4}$$

Then the flow rate of recirculation (Q_{rec}) can be calculated with V_{cp}, as follow;

$$Q_{rec} = \frac{\varepsilon(-\zeta)V_{cp}hd}{\mu L} \left[\frac{\left(\frac{h_w}{h}\right)^3 f(h_w)}{\left(\frac{h_w}{h}\right)^3 f(h_w) + \left(\frac{h_n}{h}\right)^3 f(h_n)} - \frac{h_w}{h} \right]. \tag{S5}$$

σ_{OLC}s are calculated from the slope of overlimiting current regime in I-V plot. In this work, current values at V_{app} = 8 V and 5 V are selected for this calculation.

SI Note 4. Experimental methods

Device fabrication. The presenting micro/nanofluidic devices are fabricated with minimum lithographical techniques. The building block is low cost polydimethyl-siloxane (PDMS, Sylgard 184, Dow corning, USA). Curing agent with PDMS of 1:10 is mixed and degas for an hour. After the mixture pours onto a lithographically constructed Si wafer, it cures at 75 °C for 4 h. The demolded PDMS block and Nafion (Sigma-Aldrich, USA)-patterned glass substrate are irreversibly adhered by O_2 plasma treatment (Cute-MP, FemtoScience, Korea) under microscopic alignment. The Nafion is patterned by the surface patterned method [3].

The main microchannel (1 mm (width) × 6 mm (length) × 7.5 μm (depth)) has 66 of micro-fin structures (7.5 μm (width) × 2.5 mm (length) × 7.5 μm (depth)) whose spacing define as h_w and h_n. While most of previous work [4] utilized the case of $h_w = h_n = h$, here we test pairs of (h_w , h_n) as (7.5, 7.5), (8.5, 6.5), (9.5, 5.5), (10.5, 4.5) and (11.5, 3.5). Due to $h_w + h_n$ is fixed to 15 μm, the cross-sectional area (A) and perimeter (l) of microchannel surface area are kept being constant, maintaining the identical surface and bulk conduction. For more non-uniform cases shown in Figure 4(b), the wide channel of 10.5 μm (width) and the narrow channel of 4.5 μm (width) are consecutively arranged, for example, *wwwnnn* and *wwwwwnnnnn*. In these cases, A and l are still kept being a constant. KCl electrolyte solution of 1 mM (Sigma Aldrich, USA) is injected in both main and buffer microchannel. For easy handling of solution exchange and flushing, air valves at the side microchannels are used [5].

Electrical measurement. Using Ag/AgCl electrodes, current-voltage responses are obtained by a source measure unit (Keithley 236, USA) and Labview program. An external voltage (V) ranges from 0 V to 8 V at 0.2 V/sec is applied to the main microchannel, while buffer microchannel is electrically grounded. For current-time responses, constant voltage of 5 V, which lies in the range of overlimiting current regime, is applied for 1,000 minutes by a source

measure unit. The data are collected every 1 minute.

Flow visualization. For the visualization of recirculating flow, the mixture of 1 mM KCl with sulforhodamine B (50 nM, Sigma Aldrich, USA) as a fluorescent tracer and ultrasonicated oil droplets (Canola oil, Wesson, USA) as a flow tracer are injected to both microchannels. Since oil is non-polar fluid with a low surface potential so that one can minimize the electrophoretic effect [6]. Canola oil is sonicated for 5 minutes to form oil droplets of diameter ~1-2 μm. The propagations of depletion zone and particle tracking for internal recirculation flow are imaged by an inverted fluorescent microscope (IX73, Olympus) and Micro-Manager. Conventional monodispersed micro-particles are unsuitable tracers in this experiment, since their high surface charge hinders the recirculating by high electrophoretic mobility and entering the ion depletion zone. Such aspect is actively utilized in bio-molecular preconcentration mechanism [3, 7] which is out scope of this work.

Anti-crystallization. For the demonstration, each channel compartment is designed to be 1 mm in width, 6 mm in length, and 15 μm in depth and the main channel consists of 23 microchannels that are separated by micro-fin structures between them. The width of two adjacent microchannels, h_w and h_n, are adjusted to impose non-uniformity on the array: $h_w = h_n$ = 22.5 μm (uniform) or h_w = 31.5 μm and h_n =13.5 μm (non-uniform). Note that the width and the depth of the microchannels are ~ O(10) μm and EOI is still negligible. As a crystallizable ionic species, the microchannel network is filled with calcium chloride ($CaCl_2$) solution under the consideration that it is one of the most common sources of precipitation scaling[8, 9]. Its concentration, 10 mM, is supposed to be a representative of natural seawater condition. The calcium ions ambient in the electrolyte may form calcium hydroxide ($Ca(OH)_2$) which is an inorganic compound and slightly soluble in water (solubility ~23 mM at 20 °C).

SI Note 5. Example: Variation of non-uniformity

One may extract a scaling law between geometric non-uniformity and σ_{OLC}, if one can setup a proper measure of the non-uniformity. One example of modifying non-uniformity is implemented by fabricating repeated wide or narrow channels indicated as *w* and *n* shown in SI Figure 4. As demonstrated, uniform case has the lowest σ_{OLC}, while strong non-uniform case has the highest σ_{OLC}. As the non-uniformity decreases in repeated configuration, σ_{OLC} is significantly reduced because either *nn* pairs or *ww* pairs contribute as uniform arrays. Note that the bulk and surface conduction are kept constant to allow proper comparisons in all cases. See the supporting video for the propagation of depletion zone in each configuration.

Depletion zone propagation		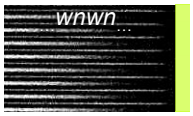		
σ_{OLC} (nS)	0.58	1.99	1.69	1.49
OLC at 10 V (nA)	9.59	27.02	25.38	23.05

SI Figure 4. Depletion zone propagation and experimentally measured σ_{OLC}s in repeated wide or narrow channels.

SI Note 6. Details of Q_{res} calculation

While the particle velocities in narrow (u_n) and wide (u_w) channel are given by $Q_{rec}/h_n d$ and $Q_{rec}/h_w d$ in the theoretical analysis, experimentally measured u_n and u_w should include electrophoretic motions (u_{EPH}) as shown in SI Figure 5. Then we have two equations ($u_n = Q_{rec} / h_n d - u_{EPH}$ and $-u_w = -Q_{rec}/h_w d - u_{EPH}$) and two unknowns ($Q_{rec}$ and u_{EPH}). First of all, u_{EPH}s obtained in this way are in the range of 4.5~12 μm/s and corresponding zeta potential of these oil droplets is in the range of -7.5 ~ -20 mV by Smoluchowski velocity equation. These values allow the droplets enter the depletion zone, which is our intention to use the oil droplet as a tracer. If the zeta potential of a tracer is relatively high, all of the tracers should escape from the non-uniform fins as similar as uniform case. Maximum tolerance of zeta potential is ~ -110 mV in this work so that regular polystyrene particle of -50 mV is not suitable tracers in this work. In addition, the range is in-line with the value of u_{EPH} (-20 mV) obtained in the uniform channel case.

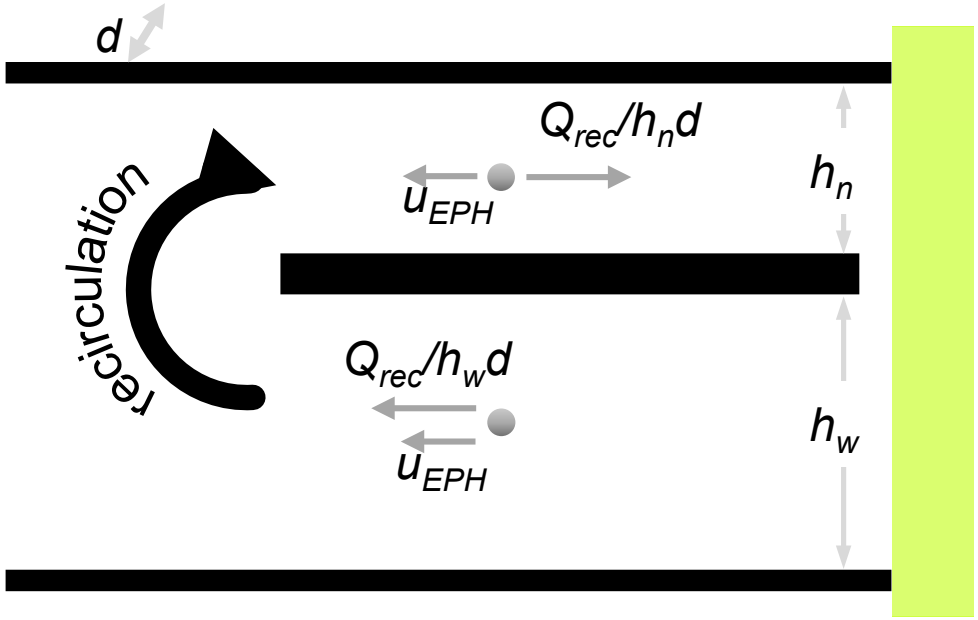

SI Figure 5. Diagram of experimentally measured velocity components in each channel.

SI Note 7. The ratio of energy needed to sustain the flow to the electric energy

The ratio is calculated as

$$\frac{\text{flow energy}}{\text{electric energy}} = \frac{\Delta P Q_{net}}{IV} = \frac{12L\varepsilon(-\zeta)|\mathbf{E}|\dfrac{h}{h_w^{\,3} f(h_w) + h_n^{\,3} f(h_n)} Q_{net}}{IV}$$

$$= \frac{12\left(2.5\times10^{-3}\right)\left(80.36\times8.85\times10^{-12}\right)(0.1)\left(\dfrac{5}{6\times10^{-3}}\right)\left(\dfrac{15\times10^{-6}}{\left(10.5\times10^{-6}\right)^3 0.2859 + \left(4.5\times10^{-6}\right)^3 0.6255}\right)\dfrac{7.0286\times10^{-14}}{60}}{\left(1.2362\times10^{-8}\right)5}$$

$$= \frac{8.053\times10^{-14}}{6.181\times10^{-8}} = 1.303\times10^{-6}$$

where h_w [m]= 10.5×10^{-6}, $f(10.5)$= 0.2859, h_n [m]= 4.5×10^{-6}, $f(4.5)$=0.6255, ε [F/m]= $80.36\times8.85\times10^{-12}$, E [V/m]= $5/(6\times10^{-3})$, ζ [V]= 0.100 and L [m]= 2.5×10^{-3}.

REFERENCES

1. Kwon, S.; Lee, H.; Kim, S. J. Elimination of pseudo-negative conductance by coercive steady state in perm-selective ion transportation. *Biomicrofluidics* **2020,** 14, (1), 014106.
2. Moya, A. A.; Belashova, E.; Sistat, P. Numerical simulation of linear sweep and large amplitude ac voltammetries of ion-exchange membrane systems. *J. Membr. Sci.* **2015,** 474, 215-223.
3. Son, S. Y.; Lee, S.; Lee, H.; Kim, S. J. Engineered nanofluidic preconcentration devices by ion concentration polarization. *BioChip Journal* **2016,** 10, (4), 251-261.
4. Kim, K.; Kim, W.; Lee, H.; Kim, S. J. Stabilization of ion concentration polarization layer using micro fin structure for high-throughput applications. *Nanoscale* **2017,** 9, (10), 3466-3475.
5. Kim, J.; Kim, H.-Y.; Lee, H.; Kim, S. J. Pseudo 1-D Micro/Nanofluidic Device for Exact Electrokinetic Responses. *Langmuir* **2016,** 32, (25), 6478-6485.
6. Moreira de Morais, J.; David Henrique dos Santos, O.; Delicato, T.; Azzini Gonçalves, R.; Alves da Rocha-Filho, P. Physicochemical characterization of canola oil/water nano-emulsions obtained by determination of required HLB number and emulsion phase inversion methods. *Journal of dispersion science and technology* **2006,** 27, (1), 109-115.
7. Zangle, T. A.; Mani, A.; Santiago, J. G. Theory and experiments of concentration polarization and ion focusing at microchannel and nanochannel interfaces. *Chem. Soc. Rev.* **2010,** 39, 1014-1035.
8. Goh, P.; Lau, W.; Othman, M.; Ismail, A. Membrane fouling in desalination and its mitigation strategies. *Desalination* **2018,** 425, 130-155.
9. Warsinger, D. M.; Swaminathan, J.; Guillen-Burrieza, E.; Arafat, H. A. Scaling and fouling in membrane distillation for desalination applications: a review. *Desalination* **2015,** 356, 294-313.